Check for updates

Received: 9 July 2021 | Revised: 13 December 2021 | Accepted: 14 December 2021

DOI: 10.1002/chir.23409

RESEARCH ARTICLE

Chirality WILEY

Tunable induced circular dichroism in gels

Yu Xue[1] | Natalie Fehn[1] | Viktoria Katharina Brandt[1] | Michele Stasi[2] | Job Boekhoven[2] | Ueli Heiz[1] | Aras Kartouzian[1]

[1]Lehrstuhl für Physikalische Chemie, Technische Universität München, Munich, Germany

[2]Department of Chemistry, Technische Universität München, Munich, Germany

Correspondence
Aras Kartouzian, Lehrstuhl für Physikalische Chemie, Technische Universität München, Lichtenbergstr. 4, Munich 85748, Germany.
Email: aras.kartouzian@mytum.de

Funding information
Deutsche Forschungsgemeinschaft, Grant/Award Number: HE 3454/21-2

Abstract

The ICD phenomenon has drawn a lot of attention in recent years in applicable fields such as chiral sensing and chiroptical devices. In this work, we first gaze at the issues of thin spin-coated films not being able to deliver consistent ICD signals. A hypothesis of the underlying problem is proposed through a brief elucidation of the spin-coating process. To confirm and eliminate the uncontrollable dynamic factors with spin coating, we then dedicate our efforts to develop a new gel system based on chiral L-/D-N′,N′-Dibenzoyl-cystine. Achiral dye molecules are intercalated in a DBC gel through a "one-step" preparation procedure. Compared to the former spin-coating system, significantly improved reproducibility of the new gel system is demonstrated. Besides, the ICD signals can be customized in a broad spectral range (wavelength tunability) by substituting dye molecules. Finally, we discuss the potential applications of this interesting system.

KEYWORDS

chiral gels, chirality transfer, induced optical activity, optically active dyes, wavelength tunability

1 | INTRODUCTION

Induced circular dichroism (ICD) describes the phenomenon in which an achiral chromophoric compound shows optical activity due to molecular interactions with chiral compounds in proximity. It is one of the chiroptical techniques which can be used to elucidate structural information complementary to NMR and X-ray.[1] It is especially powerful to determine the absolute configurations and conformations[2–5] and to probe the molecular orientations in a complex.[6,7] In recent years, ICD has drawn a lot of attention due to its potential applications, such as in the field of new materials,[8] heterogeneous catalysis,[9] drug delivery,[10] chiral nanoarchitectures,[11] and electroptical devices. Especially, thin films of molecular aggregates with π-conjugation have inspired a plethora of scientific investigations.[12]

In a previous work, we generated ICD signals of achiral rhodamine 110 in thin films with 1,1′-Bi-2-naphthol (BINOL) using a spin-coating technique.[13] In spin-coated films, rhodamine 110 preferably forms J -aggregates in the spatial vicinity of BINOL, which serves as chiral seeds and increases the possibility of rhodamine 110 to form one enantiomeric J-aggregate over its counterpart. To explore the dependency of optical activities (OA) on the relative ratio between BINOL and rhodamine, we defined the weight ratio R as $\frac{m_{BINOL}}{m_{rhod}}$, where m is the mass per volume in ethanol of the corresponding components mixed in the coating solution. The concentration of rhodamine 110 remains constant at 11.7×10^3 wt%, while weight

This is an open access article under the terms of the Creative Commons Attribution-NonCommercial License, which permits use, distribution and reproduction in any medium, provided the original work is properly cited and is not used for commercial purposes.
© 2022 The Authors. *Chirality* published by Wiley Periodicals LLC.

ratio R varies with the concentration of BINOL. When R is close to zero (R = 0.22, $m_{rhod} = 11.7 \times 10^3$ wt% with $m_{BINIO} = 2.574 \times 10^3$ wt%), the ICD maxima of one enantiomer reaches up to +250 mdeg. When more BINOL is added, that is, R increases (R = 0.67), rhodamine 110 forms smaller J-aggregates with more BINOL in the vicinity and the CD shrinks drastically to +30 mdeg, since BINOL hinders the formation of rhodamine J-aggregates.[13] Although these results clearly demonstrate the tunability of ICD in spin-coated films, great care needs to be taken when generating similar ICD curves with identical absorptions through the spin-coating technique. Multiple factors such as spinning rate[14] and spinning direction[15,16] play their role in the process. Also, numerous dynamic factors play a role during the coating process in a time scale of seconds, making the process difficult to control.

The spin-coating process is a complicated dynamic process, which can be generally divided into three stages (a) Spin-up stage: A certain amount of solution is deposited on the substrate, as the top of the fluid layer exerts the inertia and keeps the rotational speed unchanged for a short time, the bottom of the wafer rotates faster and faster. Eventually, the excess of the fluid is spun off, and the remaining fluid can co-rotate with the wafer; (b) spin-off stage: During this time, the rotating speed is kept constant, and the fluid viscous forces dominate the thickness of the film; (c) solvent-evaporation stage: The rotating speed is constant. Evaporation of solvent at this stage dominantly controls the thinning process of the film. At this point, the coating solutions effectively "gels" as the solvent evaporates rapidly. The remaining fluid's viscosity is highly probable to rise and freeze the solute in place.[17]

The overlap of the last two stages results in a complicated model of describing the thinning behavior. For instance, the changing rheological properties during the evaporation of solvent lead to the drastic change in the thinning rate of the film.[18] According to literature[19,20] during the spin-coating process, the solvent is rapidly removed from the top fluid-air interface. Therefore, a concentration gradient of solute occurs, being prone to form a solid-skin layer in the sol–gel-like fluid. Haas and Quihada[21] have stated that this skin layer could act as a barrier to further evaporation of the rest of the fluid, making the dynamics in this process complicated to predict, even more complicated if we also take the diffusivity of the solute and solvent into consideration. During the spin-coating process, plenty of dynamic factors interact with each other in a short time scale. Therefore, the spin-coating process is considered one of the non-equilibrium processes that do not allow the molecular favored state of solutes. For ICD experiments with BINOL and rhodamine 110, this issue was strongly reflected in the reproducibility of the samples.

Nevertheless, one of the dominating advantages of spin-coating in this regard is that it offers an extensive range of potential material properties under a given material composition.[22]

Here, we have developed a new system in which ICD can be studied based on the chiral low molecular weight gelator (LMWG) N′,N′-dibenzyol-cystine (DBC). Upon protonation of the di-acid DBC, it assembles and forms a rigid three-dimensional fiber network that immobilizes its fluid by capillary forces and surface tension.[23,24] Non-covalent interactions, such as π- π interactions, H-bonds, and van-der-Waals interactions, are crucial for the self-assembly.[25] In principle, this process is thermo-reversible; that is, the gel will transform into a transparent solution beyond a specific temperature, below which the solution will slowly gelate back to a gel. This temperature is defined as $T_{sol-gel}$,and, in the case of DBC, it is concentration dependent. For concentrations used in this work, it is slightly lower than the boiling temperature of water ($T_{sol-gel}$ = 365–366 K < 373 K) [26]. Accordingly, an aqueous solution of DBC can be heated up above the $T_{sol-gel}$ of DBC without causing the solution to boil, and thus, the gel can be annealed. This process provides enough thermal energy to the dynamic self-assembly of DBC gel so that the equilibrium configuration can be achieved. In this regard, a gel system holds an intrinsic advantage of generating reproducible signals over a spin-coated system. DBC is considered as a perfect candidate for being one of the chiral LMWGs and showing good water solubility.

2 | MATERIALS AND METHODS

N′,N′-dibenzoyl-L-Cystine (L-DBC) is commercially available from *Sigma-Aldrich;* its enantiomer (D-DBC) is not commercially available and was synthesized following the recipes available in the literature (Scheme 1).[27,28] Briefly, D-Cystine (500 mg, 2 mmol) is dissolved in a biphasic mixture of diethyl ether (2 ml), NaOH 2 M (4.6 ml), and ethanol (200 µl). The solution is cooled to 0°C, and an additional 6.25 ml of water is added. Benzoyl chloride (730 µl, 4.3 mmol) is added dropwise under stirring. The solution is warmed to room temperature and stirred overnight. The mixture is diluted with water and acidified to pH 2 with 6 M HCl. Then, the white solid is filtered under vacuum and washed with hot water. The product is further purified via preparative HPLC (H_2O:TFA 1%/ACN: TFA 1%). The product is a white powder (730 mg; 81% yield). L-DBC and D-DBC are used to form the gel.

The employed dyes are all purchased from *Radiant Dyes Laser Accessories GmbH* (see Schematic S1). Analytical grade ethanol (>99.5) is purchased from *Carl Roth*. All chemicals are used without further purification.

SCHEME 1 Synthesis diagram of D-DBC[27,28]

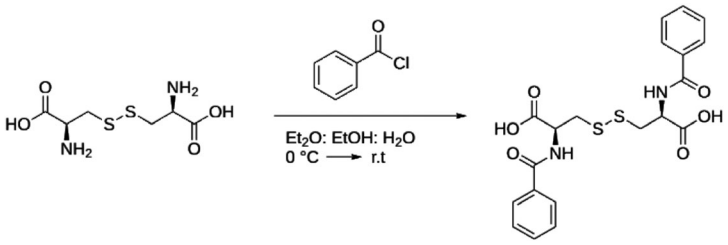

Figure 1 lists the preparation steps. The aqueous dye solution is added to 10 mM DBC solution, prepared ahead of time by dissolving the DBC in 200 mM MES buffer with pH of 6. Table 1 shows the concentration of the dye solution, which is calculated based on their molar absorptivity. Table 1 also lists different volumes of dye solutions added to the DBC solution not to saturate the spectrometer and generate the optimal absorption signals.

After the dyes are well dispersed in the sample, we add 1 M HCl to induce the gelation process. In our case unless expressly stated, 105 μl of 1 M HCl is added for 1 ml sample. Now annealing is conducted to generate uniform and stable gels, where the samples are heated up to at least the $T_{sol-gel}$ and the gel completely transforms into a transparent solution. The mixture needs to be transferred into a cuvette for measurements immediately before it gelates in the vial. Afterwards, the solution is slowly cooled down to room temperature and transforms back into gel again.

All studied gel samples are analyzed by a Jasco J-815 CD Spectrometer. The absorption and CD measurements are performed in the wavelength range between 300 and 700 nm with the scanning speed of 20 nm/min. During the measurements, the data pitch is 1 nm with standard sensitivity.

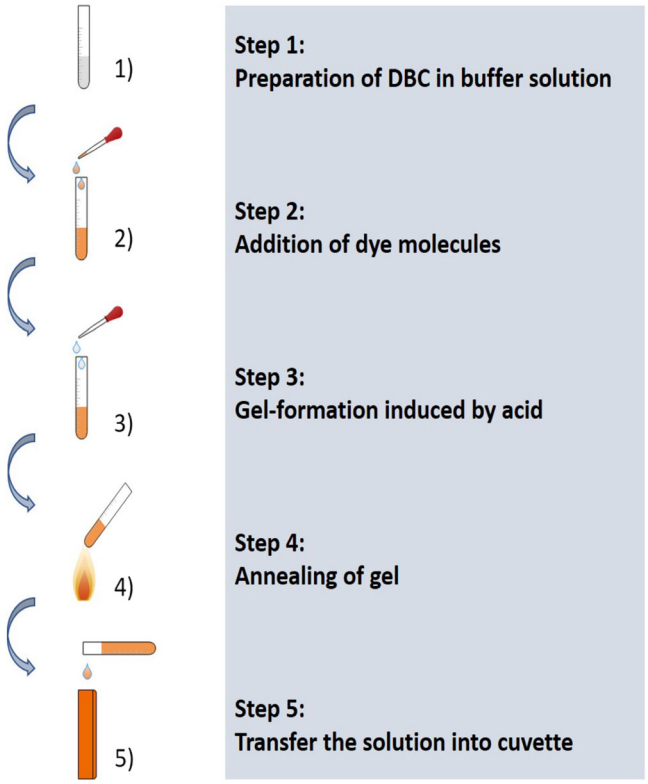

FIGURE 1 Preparation procedure of samples, where dye molecules are intercalated in DBC gel

3 | RESULTS AND DISCUSSION

3.1 | Reproducibility

Our first goal was to obtain a more reproducible system to induce CD into dye molecules compared to spin-coated thin films. In order to demonstrate the situation with ICD in spin-coated films, Figure 2A depicts the absorption and CD spectra of nominally identical spin-coated samples.

In this case, the absorption curves are similar in intensity and band positions; however, the ICD curves differ to a great extent. As already mentioned in the previous section, the reason behind this is speculated to be the randomly distributed molecular states of the rhodamine 110 aggregates. The mobility of the dye and BINOL molecules in the solution is relatively high, and they quickly change their neighbors so that on average no induced CD can be observed in the solution.[13] After the solvent (ethanol) spins off and evaporates, the remained rhodamine and BINOL are frozen at a random non-equilibrium molecular configuration,[22] which results in irreproducible ICD signals. Even minute control of spin-coating parameters such as temperature, rotation speed, rotation time, solution concentration, and solution injection speed could not guarantee for reliable and reproducible sample fabrication with regard to ICD.

Figure 2B demonstrates the spectral curves of rhodamine 110 as it is intercalated in DBC gel. There are seven samples measured. Five of them are the replicates of rhodamine 110 in L-DBC gel and one sample for D-DBC and the racemic mixture of DBC each. The absorption curves of all seven samples are identical. Two bands appear, one

TABLE 1 Concentrations of dye solutions regarding their molar absorptivity and added amount in the samples

	Molar absorptivity $\times 10^4$ ($Lmol^{-1}cm^{-1}$)[25]	Con. (mg/ml)	Vol (μl) added per 1 ml
Rhodamine 110	8.99	3.33	30
Uranine	9.92	3.39	30
Furan 2	7.79	8.58	30
Nile blue	7.75	4.40	50
Cresyl violet Perchlorate	6.74	4.38	30

with a broad absorption band between 450 and 550 nm, with the maximum at 503 nm and a shoulder at 472 nm. The second one shows lower intensity from 300 to 350 nm with a peak at 330 nm, resulting from the S2 ← S0 transition of rhodamine 110.[13]

CD curves of rhodamine 110 in L-DBC display broad ICD signals from 420 to 550 nm, with a vague double-peak feature at 495 and 517 nm. The positive OAs reach a maximum of 20 mdeg. This behavior is mirrored for D-DBC, and OAs of rhodamine 110 in racemic DBC are zero. The five resembling ICD curves of rhodamine 110 in L-DBC, and the mirrored curve of rhodamine 110 in D-DBC, demonstrate the excellent reproducibility of our new gel system. The dominating mechanism here is speculated to be the DICD; that is, the ICD is induced by the interaction of chiral DBC and achiral rhodamine 110 via perturbation of the transition dipole moments in the dye molecule, which is supported by the fact that the ICD curves are not bisignate.

Since thin layers of gel with dye molecules, embedded between glass slides, exhibit the same features and behavior as the gels in cuvettes (see Figure S1), we focus here on the discussion of the latter. We would like to point out, however, that there are reports on molecular aggregation both being similar and different for the solid and liquid state, respectively.[29,30]

Compared to the spin-coated rhodamine 110 with BINOL, rhodamine 110 intercalated in DBC has shown high reproducibility in both absorption curves and ICD signals. Besides, it is also noteworthy that the ICD intensities for both systems differ in magnitude. In our previous contribution,[13] we have found that (1) the observed ICD of rhodamine 110 stems from both J-aggregates and monomers. (2) J-aggregates lead to a much stronger ICD compared to monomers. (3) The more extended the chains of J-aggregates, the larger the ICD signals. (4) ICD signals are significantly susceptible to the relative concentration ratios between rhodamine 110 and BINOL molecules. In the case of DBC-gel, we have revealed in the past that the expected molecular arrangement of DBC in gel is forming fibers.[31] There are four hydrogen bonds per unit between amino and carbonic acid moieties that form the backbone of the molecular stacks. Confocal microscopy images reveal that the majority of dye molecules are located around the resulting fibrous structures of the gel (see Figure S2). In contrast, we do not observe many dye molecules in the space between gel fibers where the solvent, that is, water, is retained by the gel, which is the case for all the five considered dyes in the present work. This leads us to the conclusion that the dye–gel interaction is favored over dye–dye or dye–water interactions. A reasonable option for dye accommodation, along the gel backbone, can be the cavity between the phenyl moieties of two neighboring DBC molecules (see Figure S2). With the molecular structures of DBC and dyes in mind, the interactions between the two entities appear to be π-stacking also. In the following, we regard to the described positions within the structure of the gel backbone for dye molecules as cavities and the process of occupying these as intercalation. The cavity is proposed to be able to accommodate only one dye molecule. Therefore, we assume that the ICD effects are mainly induced based on the monomers' level. ICD signals emerging from DBC gel are estimated to be weaker than those from spin coating, supported by the observations in Figure 2A,B. Furthermore, the ICD's dependency on the concentration is likely to be less sensitive, as the monomers in the cavity would not be affected when the content of chiral DBC varies (see Figure S3).

3.2 | Wavelength tunability

After demonstrating the excellent reproducibility of gel-based ICD, we now focus on the tunability of this system. The tunability of ICD signals in a wide spectral range is explored by substituting various dyes in the chiral DBC. We want to introduce a specific example to illustrate how the ICD signals can be tuned by changing the dyes in chiral DBC. The same method is applied; instead of rhodamine 110, we intercalate cresyl violet perchlorate as the achiral dye in chiral DBC gel.

As Figure 3 depicts, a broad absorption band with two maxima at 512 and 570 nm occurs, which is different

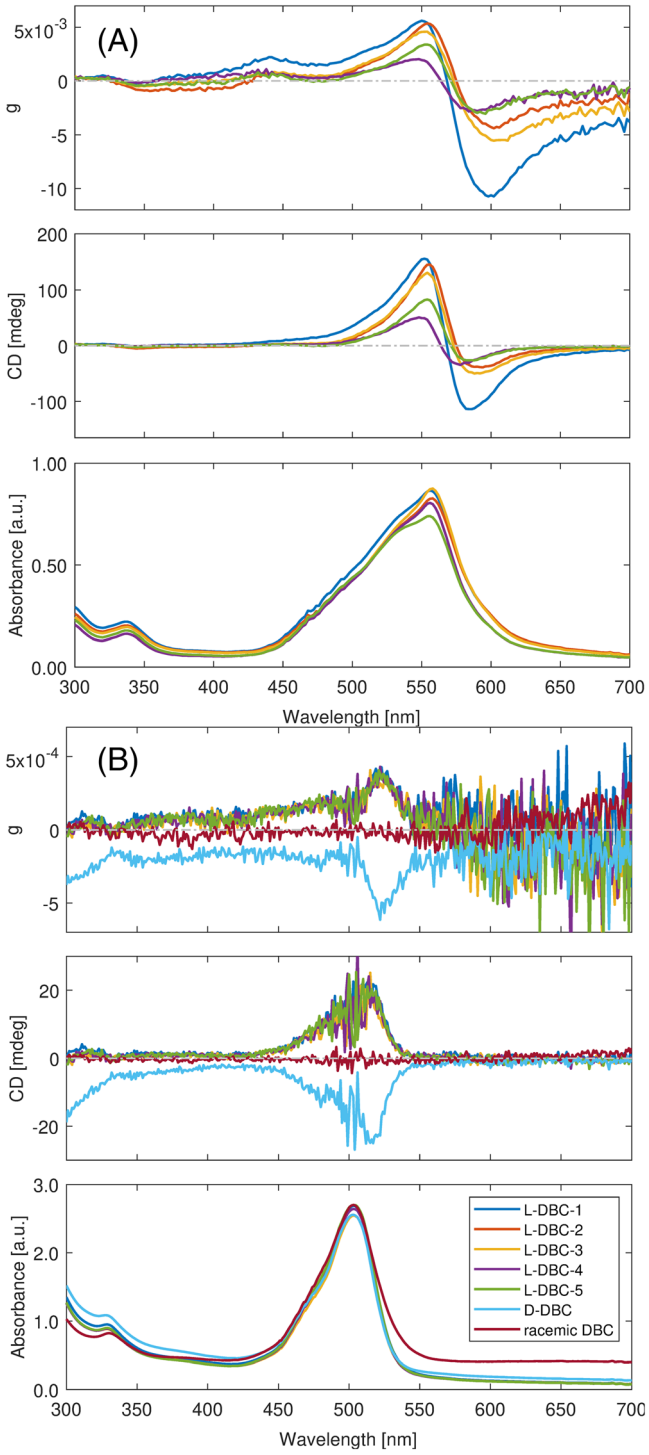

FIGURE 2 (A) Rhodamine 110 and BINOL were spin-coated on the substrate with a rotation speed of 960 rpm. The various spectra are recorded for nominally identical samples, where all the controllable parameters have been kept identical; (B) rhodamine 110 is intercalated in DBC-gel. Five replicates of samples in L-DBC (positive ICD), one replicate in D- DBC (negative ICD), and one sample in the racemic mixture (optically inactive) were prepared

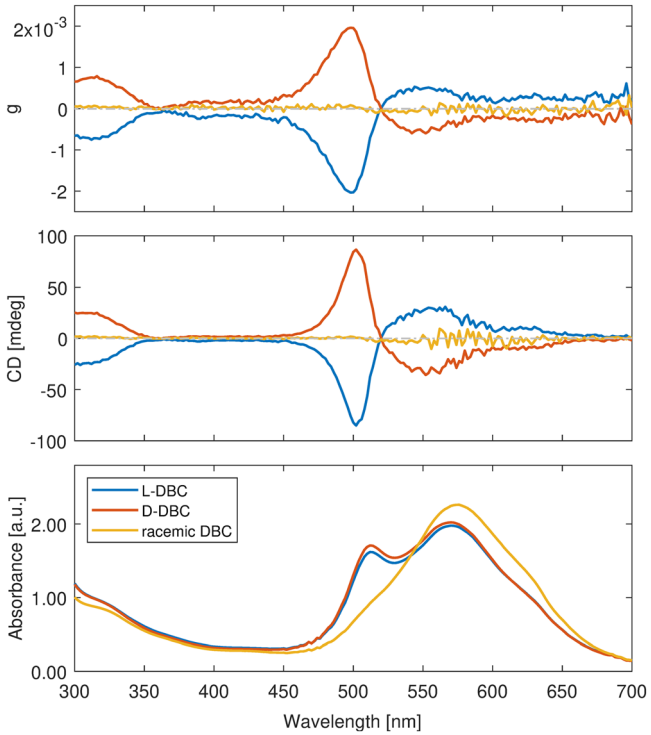

FIGURE 3 Cresyl violet perchlorate intercalated in the L-DBC, D-DBC, and racemic DBC gel

from the transitions of rhodamine 110. Accordingly, ICD signals in the corresponding wavelength range are observed. The absorption patterns stay identical for the opposite pure enantiomers. However, for the racemic mixture, the second peak located at 512 nm, which can be assigned to the H-aggregates of this dye,[32–34] has vanished, and the first peak has shifted to a higher wavelength of 574 nm. As for ICD signals, they show bisignate features for the aggregate band, as expected from the exciton coupling model[35] and stay positive, between 520 nm and the cutoff range 700 nm, with a maximum of 30 mdeg. A zero-crossing occurs at 522 nm, and OAs reach a negative maximum of −97 mdeg at 503 nm. The opposite enantiomer D-DBC displays the mirror image ICD spectrum while for the racemic mixture no ICD is observed. The difference in absorption features for pure enantiomers and racemic mixture reveals that these molecules do not form H-aggregates in the case of the racemic gel structure in contrast to the enantiopure samples. This suggests that the intermolecular interactions are not independent of the gel structure. In the racemic mixture, as the hypothesis addressed earlier, one cresyl violet perchlorate molecule is situated within one cavity of the chiral DBC gel. Impacts from the opposite enantiomer

within the close vicinity might counterbalance the original molecular orientation and disfavor the formation of aggregates across the cavity borders.

We have shown the spectral results of rhodamine 110 and cresyl violet perchlorate separately. For a better demonstration of tunable ICD in the spectral range, we have chosen another three achiral dyes: furan 2, uranine, and nile blue, together with rhodamine 110 and cresyl violet perchlorate, whose absorptions span from 300 to 700 nm. Figure 4 shows the spectral results of each dye in L-DBC, while the optical response of the dyes in D-DBC can be found in Figure S4. All five dyes have different transitions, and their ICD signals differ from each other in terms of position, sign, and intensity. Thus, we have successfully generated an extensive range for the wavelength tunability of ICD by substituting different dyes in chiral DBC.

So far, we only introduced a single type of dye in one sample, which only enables the ICD signals to stem from the transition of one kind of dye molecule. Since only one dye molecule can be accommodated in a cavity, using pairs or trios of dyes in a single sample should produce a simple superposition of the ICD spectra of the individual dyes, unless the dye molecules could communicate across the cavities. Using pairs and trios of dyes that are intercalated in DBC gel would thus provide us with a more versatile wavelength tunability (Figure 5).

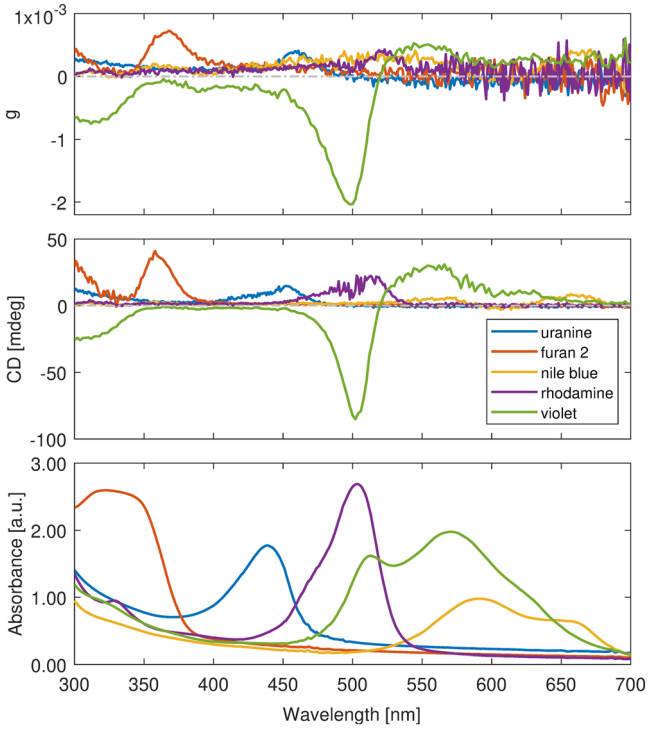

FIGURE 4 Broad additive spectral range of tunable ICD signals by intercalating uranine, furane 2, nile blue, rhodamine (110), and violet (cresyl violet perchlorate) in L-DBC

Figure 5A shows the mirror image of both uranine and rhodamine 110 intercalated in L-DBC and D-DBC. Figure 5B demonstrates the spectral results of the mixture consisting of uranine, cresyl violet perchlorate, and nile blue. We have mathematically summed the spectral results of each individual dye together and compared

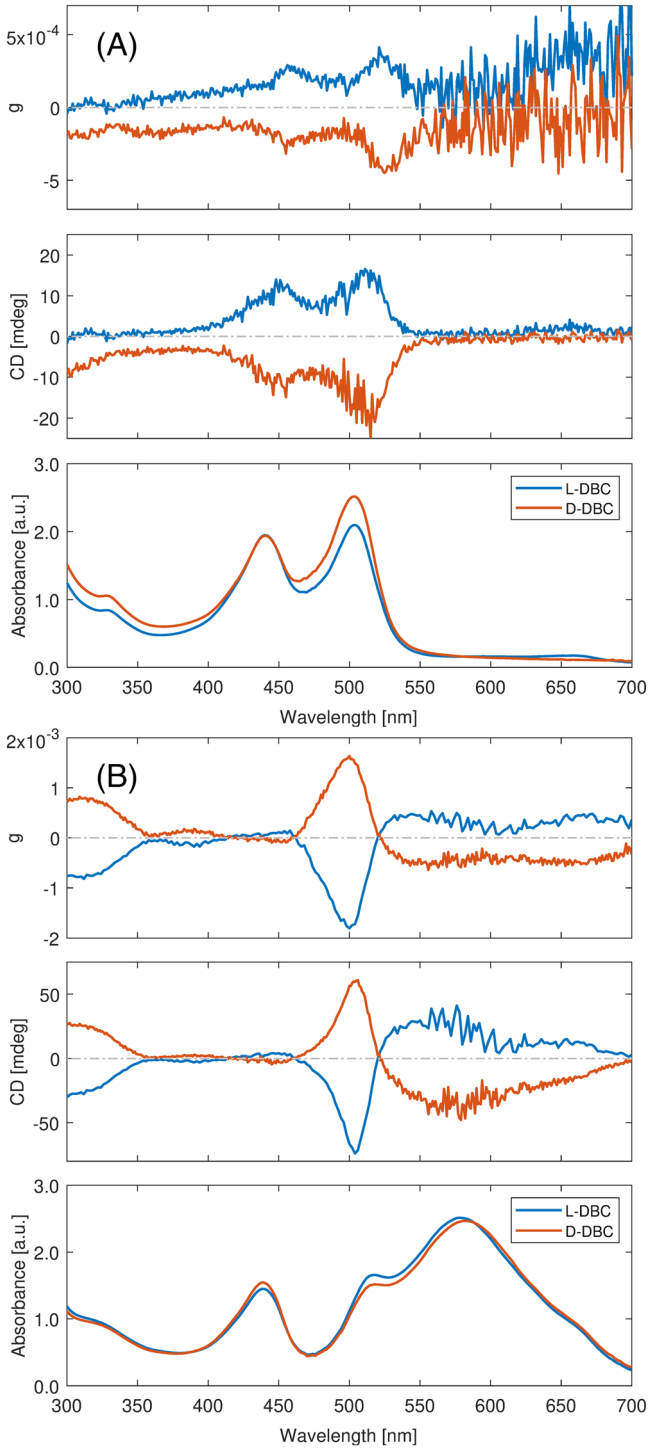

FIGURE 5 Simultaneous induced CD in multiple dyes. (A) For a pair of dyes; uranine and rhodamine 110; (B) for a trio of dyes: uranine, cresyl violet perchlorate, and nile blue

them with the experimental result of the mixed sample (see Figure S5). We have found that ICDs occur in the absorption ranges of both dyes. In general, the remarkable resemblance between mathematically summed and experimental curves can be observed for both absorption curves and ICD signals, which indicates that the overall ICD signals are the accumulative results of optical activity arising from every single dye. Therefore, the co-existence of multi-dyes in chiral DBC gel does not have additional impacts on each dye's transition dipole moments. However, there are examples in which the co-existence of multi-dyes impacts the transition dipole moments, which results in variations in absorption and ICD signals (see Figure S6).

4 | CONCLUSION AND OUTLOOK

At first, we confirmed our hypothesis that spin-coated thin films generate inconsistent ICD signals. The spin-coating process freezes the solutes in the films at non-equilibrium states due to the complicated dynamic processes in the limited time scale. Starting from there, we dedicate this work to develop a new system based on chiral DBC gel. The gel's advantage is that the preparation procedure provides enough thermal energy and time, which allows the achiral molecules to reach their favored molecular states through annealing (ramp-up) and to keep these equilibrium states as it cools down to room temperature (ramp-down). We demonstrate excellent reproducibility by comparing the spectral results of rhodamine 110 in spin-coated and gel systems. Achiral dye molecules are intercalated in the chiral DBC gel through a simple "one-step" preparation procedure. For demonstrative purposes, we chose five achiral dyes to represent the excellent tunability of this system, including wavelength and intensity tunability. Other dyes with good solubility in water can be candidates also. More achiral dye molecules can be applied to generate more accurate and concrete tuning of the ICD signals. Besides, tunability can be expanded and refined by intercalating more than one dye in the gel.

In spin-coated films, ICD signals of achiral dyes are often generated by the aggregates. Due to the specific property of gel DBC, one dye molecule is speculated to fit in one cavity in the gel, the so called "one molecule per site." This interacting nature between achiral dyes and chiral gelator determines that there is a less susceptible dependence on the concentration. However, the observations from the racemic mixture, showing different absorptive properties than the pure enantiomer in the case of cresyl violet perchlorate, suggest the occurrence of interactions (e.g., aggregation of the dye molecules) across the cavities, which cannot be fully neglected and requires further analysis of the enantiomeric dependence of the structure of the DBC gel fibers. It is noteworthy that the spectra recorded for cresyl violet perchlorate samples before gelation show that the aggregation behavior of the dye molecules is independent of the enantiomeric state of the solution (see Figure S7).

Chiral assemblies with controllable ICDs open up new perspectives in the field of chiroptical applications, including but not limited to optical amplifier materials,[23,36,37] chiral sensing,[38,39] optical switch, and data storage applications.[40–42] Furthermore, a research group in Spain has shown that the supramolecular gels can be applied as organic reaction media.[43] Such a gelated system holds intrinsic advantages over traditional reaction media (e.g., self-assembly nature, the capability of immobilizing solvents within the networks, sensitivity to external stimuli, abundant interfaces between formed nanofibers, and liquid phase). A system with tunable ICD responses can be utilized as photo-sensitive reaction chambers. Alternatively, in the field of heterogeneous asymmetric catalysis, chirality can be successfully transferred between chiral and achiral components in the gel. Hence, this gel system can provide a platform for the actual catalyst (e.g., metal clusters) to gain a sense of chirality, enhancing the stereoselectivity of the final product.[44] Once the formed supramolecular assemblies of chiral and achiral compounds are well understood, it is highly possible to fine-tune the catalysis' performance to increase its efficiency. Furthermore, due to the simple sol–gel transition, the recovery process of the catalyst is much easier. The catalyst can be collected simply by filtration.

ACKNOWLEDGMENTS

The authors are thankful to J. Rodon-Fores for recording the confocal microscopy images. N.F. would like to thank Studienstiftung des Deutschen Volkes for financial support and enriching experiences (Deutsche Forschungsgemeinschaft, HE 3454/21-2).

DATA AVAILABILITY STATEMENT

The data that support the findings of this study are available from the corresponding author upon reasonable request.

ORCID

Aras Kartouzian https://orcid.org/0000-0002-2193-2902

REFERENCES

1. Berova N, Bari LD, Pescitelli G. Application of electronic circular dichroism in configurational and conformational analysis of organic compounds. *Chem Soc Rev*. 2007;36(6):914-931.

2. Hosoi S, Kamiya M, Ohta T. Novel development of exciton-coupled circular dichroism based on induced axial chirality. *Org Lett*. 2001;3(23):3659-3662.
3. Di Bari L, Pescitelli G, Salvadori P. Conformational Study of 2,2'-Homosubstituted 1,1'-Binaphthyls by Means of UV and CD Spectroscopy. *J Am Chem Soc*. 1999;121:(35):7998-8004. https://doi.org/10.1021/ja990326b
4. Torabi Kohlbouni S, Sarkar A, Zhang J, Li X, Borhan B. Absolute stereochemical determination of 1,2-diols via complexation with dinaphthyl borinic acid. *Chirality*. 2020;32(6):817-823.
5. Górecki M, Capozzi MAM, Albano G, Cardellicchio C, Di Bari L, Pescitelli G. Stereochemical analysis of β-keto sulfoxides by circular dichroism. *Chirality*. 2018;30(1):29-42.
6. Zhang X, Nau WM. Chromophore alignment in a chiral host provides a sensitive test for the orientation—intensity rule of induced circular dichroism. *Angew Chem Int Ed Engl*. 2000; 39(3):544-547.
7. Mayer B, Zhang X, Nau WM, Marconi G. Co-conformational variability of cyclodextrin complexes studied by induced circular dichroism of azoalkanes. *J Am Chem Soc*. 2001;123(22): 5240-5248.
8. Yashima E, Ousaka N, Taura D, Shimomura K, Ikai T, Maeda K. Supramolecular helical systems: helical assemblies of small molecules, foldamers, and polymers with chiral amplification and their functions. *Chem Rev*. 2016;116(22): 13752–13990
9. Desmarchelier A, Caumes X, Raynal M, Vidal-Ferran A, van Leeuwen PWNM, Bouteiller L. Correlation between the selectivity and the structure of an asymmetric catalyst built on a chirally amplified supramolecular helical scaffold. *J am Chem Soc*. 2016;138(14):4908-4916.
10. Rajora MA, Lou JWH, Zheng G. Advancing porphyrin's biomedical utility via supramolecular chemistry. *Chem Soc Rev*. 2017;46(21):6433-6469.
11. Zhang L, Wang T, Shen Z, Liu M. Chiral nanoarchitectonics: towards the design, self-assembly, and function of nanoscale chiral twists and helices. *Adv Mater*. 2016;28(6):1044-1059.
12. Albano G, Pescitelli G, di Bari L. Chiroptical properties in thin films of π-conjugated systems. *Chem Rev*. 2020;120(18): 10145-10243.
13. von Weber A, Stanley P, Jakob M, Kartouzian A, Heiz U. Tunable Induced Circular Dichroism in Thin Organic Films. *J Phys Chem C*. 2019;123:(14):9255-9261. https://doi.org/10.1021/acs.jpcc.9b01323
14. Albano G, Salerno F, Portus L, Porzio W, Aronica LA, Di Bari L. Outstanding Chiroptical Features of Thin Films of Chiral Oligothiophenes. *ChemNanoMat*. 2018;4:(10):1059-1070. https://doi.org/10.1002/cnma.201800244
15. Yamaguchi T, Kimura T, Matsuda H, Aida T. Macroscopic spinning chirality memorized in spin-coated films of spatially designed dendritic zinc porphyrin J-aggregates. *Angew Chem Int Ed*. 2004;43(46):6350-6355.
16. Wolffs M, George SJ, Tomović Ž, Meskers SCJ, Schenning APHJ, Meijer EW. Macroscopic origin of circular dichroism effects by alignment of self-assembled fibers in solution. *Angew Chem Int Ed*. 2007;46(43):8203-8205.
17. Tyona MD. A theoritical study on spin coating technique. *Advances in materials Research*. 2013;2:(4):195-208. https://doi.org/10.12989/amr.2013.2.4.195
18. Flack WW, Soong DS, Bell AT, Hess DW. A mathematical model for spin coating of polymer resists. *J Appl Phys*. 1984; 56:(4):1199-1206. https://doi.org/10.1063/1.334049
19. Qu G, Zhao X, Newbloom GM, et al. Understanding Interfacial Alignment in Solution Coated Conjugated Polymer Thin Films. *ACS Appl Mater Interfaces*. 2017;9(33):27863-27874. https://doi.org/10.1021/acsami.7b08133
20. Bornside DE, Macosko CW, Scriven LE. Spin coating: one dimensional model. *J Appl Phys*. 1989;66(11):5185-5193.
21. Haas DE & Quijada JN. Effect of solvent evaporation rate on "Skin" formation during spin coating of complex solutions. Proceedings of the Society of Photo-Optical Instrumentation Engineers (Spie); 2000 Jan 26–28; San Jose, Ca. Spie-Int Soc Optical Engineering. p 280–284. (Proceedings of the Society of Photo-Optical Instrumentation Engineers (Spie)). https://www.spiedigitallibrary.org/conference-proceedings-of-spie/3943/1/Effect-of-solvent-evaporation-rate-on-skin-formation-during-spin/10.1117/12.384348.short?SSO=1&tab=ArticleLink
22. Chandran S, Baschnagel J, Cangialosi D, et al. Processing pathways decide polymer properties at the molecular level. *Macromolecules*. 2019;52(19):7146-7156.
23. Terech P, Weiss RG. Low molecular mass gelators of organic liquids and the properties of their gels. *Chem Rev*. 1997;97(8): 3133-3160.
24. Estroff LA, Hamilton AD. Water gelation by small organic molecules. *Chem Rev*. 2004;104(3):1201-1218.
25. Huang S, Yu H, Li Q. Supramolecular chirality transfer toward chiral aggregation: asymmetric hierarchical self-assembly. *Advanced Science*. 2021;8(8):2002132.
26. Zhong J, Fu H, Jia X, et al. A pH-/thermo-responsive hydrogel formed from N,N′-dibenzoyl-l-cystine: properties, self-assembly structure and release behavior of SA. *RSC Advances*. 2019;9:(21):11824-11832. https://doi.org/10.1039/c8ra09058k
27. Klepel F, Ravoo BJ. Dynamic covalent chemistry in aqueous solution by photoinduced radical disulfide metathesis. *Org Biomol Chem*. 2017;15(18):3840-3842.
28. Martin TA. N-acyl- and N-sulfonylcysteine derivatives. *J Med Chem*. 1969;12(5):950-953.
29. Hassan Omar O, Falcone M, Operamolla A, Albano G. Impact of chirality on the aggregation modes of l-phenylalanine- and d-glucose-decorated phenylene–thiophene oligomers. *New J Chem*. 2021;45:(27):12016-12023. https://doi.org/10.1039/d1nj02125g
30. Resta C, Pescitelli G, Di Bari L. Natural α-Amino Acid-Functionalized Poly(phenyleneethynylene)s (PPEs): Synthesis and Chiroptical Characterization of Aggregate States. *Macromolecules*. 2014;47:(20):7052-7059. https://doi.org/10.1021/ma501623a
31. Boekhoven J, Brizard AM, Stuart MCA, et al. Bio-inspired supramolecular materials by orthogonal self-assembly of hydrogelators and phospholipids. *Chem Sci*. 2016;7(9): 6021-6031.
32. Jafari A, Ghanadzadeh A, Tajalli H, Yeganeh M, Moghadam M. Electronic absorption spectra of cresyl violet acetate in anisotropic and isotropic solvents. *Spectrochim Acta a Mol Biomol Spectrosc*. 2007;66(3):717-725.
33. Banik S, Hussain SA, Bhattacharjee D. Modified aggregation pattern of cresyl violet acetate adsorbed on nano clay mineral

layers in Langmuir Blodgett film. *J Photochem Photobiol A Chem*. 2018;353:570-580.
34. Urrutia MN, Ortiz CS. Novel oxazine and oxazone dyes: aggregation behavior and physicochemical properties. *New J Chem*. 2016;40:(12):10161-10171. https://doi.org/10.1039/c6nj02053d
35. Harada N. Exciton coupled circular dichroic spectroscopy and its application to determination of absolute configuration. (Part 1) Chiroptical interaction between two or more identical chromophores. *J Syn Org Chem Jpn*. 1983;41(10):914-924. https://www.jstage.jst.go.jp/article/yukigoseikyokaishi1943/41/10/41_10_914/_article/-char/en
36. Hirahara T, Yoshizawa-Fujita M, Takeoka Y, Rikukawa M. Solvent polarity effects on supramolecular chirality of a polyfluorene-thiophene copolymer. *Chirality*. 2018;30(6):699-707.
37. Huang H, Duan H, Yin L, et al. Macromolecular chiral amplification through a random coil to one-handed helix transformation induced by metal ion coordination in an aqueous solution. *Macromolecules*. 2020;53(14):6002-6017.
38. Zuo W, Huang Z, Zhao Y, et al. Chirality sensing of choline derivatives by a triple anion helicate cage through induced circular dichroism. *Chem Commun*. 2018;54(53):7378-7381.
39. Kong XT, Besteiro LV, Wang ZM, Govorov AO. Plasmonic chirality and circular dichroism in bioassembled and non-biological systems: theoretical background and recent progress. *Adv Mater*. 2020;32(41):1801790.
40. Ohira A, Okoshi K, Fujiki M, Kunitake M, Naito M, Hagihara T. Versatile helical polymer films: chiroptical inversion switching and memory with re-writable (RW) and write-once read-many (WORM) modes. *Adv Mater*. 2004;16(18):1645-1650.
41. Muraoka T, Kinbara K, Kobayashi Y, Aida T. Light-Driven Open−Close Motion of Chiral Molecular Scissors. *J Am Chem Soc*. 2003;125:(19):5612-5613. https://doi.org/10.1021/ja034994f
42. Rodríguez R, Quiñoá E, Riguera R, Freire F. Multistate Chiroptical Switch Triggered by Stimuli-Responsive Chiral Teleinduction. *Chem Mater*. 2018;30:(8):2493–2497. https://doi.org/10.1021/acs.chemmater.8b00800
43. Escuder B, Rodríguez-Llansola F, Miravet JF. Supramolecular gels as active media for organic reactions and catalysis. *New J Chem*. 2010;34:(6):1044-1054. https://doi.org/10.1039/b9nj00764d
44. Kartouzian A. Spectroscopy for model heterogeneous asymmetric catalysis. *Chirality*. 2019;31(9):641-657.

SUPPORTING INFORMATION

Additional supporting information may be found in the online version of the article at the publisher's website.

How to cite this article: Xue Y, Fehn N, Brandt VK, et al. Tunable induced circular dichroism in gels. *Chirality*. 2022;1-9. doi:10.1002/chir.23409